PCCP

ROYAL SOCIETY OF CHEMISTRY

PAPER

View Article Online
View Journal | View Issue

Cite this: *Phys. Chem. Chem. Phys.*, 2024, **26**, 23646

Modulating molecular plasmons in naphthalene *via* intermolecular interactions and strong light–matter coupling†

Zhen Liu* and Xiao Wang *

Received 1st May 2024,
Accepted 16th August 2024

DOI: 10.1039/d4cp01816h

rsc.li/pccp

We conducted a theoretical investigation on the modulation of plasmon-like resonances in naphthalene – the so-called molecular plasmons – through intermolecular interactions and strong light–matter coupling. The configuration interaction with single excitations (CIS) approach and its quantum electrodynamics extension (QED-CIS-1) are used to describe the molecular plasmon states under these interactions. We detail the effects of changing intermolecular distances of the naphthalene dimer and incorporating the naphthalene molecule into optical cavities, both allowing for precise control of naphthalene's plasmonic responses. Our results show significant shifts of the plasmon peak in the absorption spectra of naphthalene, depending on the spatial configuration of the dimer and cavity parameters such as polarization, frequency, and coupling strength. Further investigation of the naphthalene dimer in a cavity reveals a synergistic effect on the plasmon peak when the two types of interactions are combined. This research provides insights into the plasmonic behavior of simple polyacenes like naphthalene and opens up possibilities for plasmon modulation in more complex systems.

1 Introduction

Defined as quasiparticles arising from the coherent superposition of individual electron–hole pair transitions, plasmons represent a collective excitation to the understanding of light–matter interactions. Due to their ability to strongly manipulate electromagnetic fields, plasmons have found a myriad of applications including electronics, spectroscopies, energy harvesting, and photocatalysis.[1–7] As traditional devices enter the nanoscale regime, molecular plasmonics, characterized by plasmon-like features exhibited within individual molecules, has emerged as a promising avenue for understanding and utilizing the plasmonic phenomenon in the few-atom limit.[8–10] Here, the quantum treatment of electronic excitations becomes essential, unraveling the intricate interplay between the molecular structure and the plasmonic behavior. Among the candidates for exploring molecular plasmons, naphthalene stands out as an intriguing subject of investigation. As the simplest polyacene, naphthalene serves as a building block for more complex aromatic hydrocarbons. The structural simplicity of small polyacenes has facilitated theoretical and experimental manipulation[10,11] but also provides insights into the plasmonic behavior of larger systems, such as graphene. Previous studies[12–16] have found that naphthalene exhibits distinctive optical properties, especially a strong peak called the β-peak in its optical absorption spectra. This peak arises dominantly from the constructive interaction of two single-particle transitions, which is reminiscent of plasmon-like characteristics. The ability to precisely control molecular plasmons enables the development of novel nanoscale devices with enhanced performance.

The modulation of plasmons can be achieved *via* traditional techniques such as strain, alloying, and interface engineering in order to fine-tune the optical and electronic properties of plasmonic devices.[17–20] Intermolecular interactions, which can be altered by changing the distance between plasmonic entities due to strain or other methods, have been shown to influence the characteristics of plasmonic behaviors in graphene.[21,22] Recent advancements have further expanded the toolkit for manipulating matter excitations (electronic and/or vibrational) using strong light–matter interaction.[23–27] This phenomenon, arising from the coupling between matter and light in nanoscale or microscale cavities, offers a versatile platform for controlling the properties of molecular plasmons. In this manuscript, we showcase the potential of intermolecular interactions and strong light–matter coupling for modulating molecular plasmons in naphthalene using theoretical methods.

First principles investigations play a crucial role in elucidating the mechanisms that govern molecular plasmons and their modulation. Among them, configuration interaction (CI)

Department of Chemistry and Biochemistry, University of California Santa Cruz, Santa Cruz, CA 95064, USA. E-mail: zliu373@ucsc.edu, xwang431@ucsc.edu

† Electronic supplementary information (ESI) available. See DOI: https://doi.org/10.1039/d4cp01816h

methods, particularly the CI with single excitations (CIS) approach, have been used to describe the electronic excitations underlying plasmonic phenomena.[28–30] By accounting for the interactions between electronic configurations within single-particle excitations, CIS provides a simple but valuable framework for elucidating the nature of plasmonic excited states. Moreover, the recent development of the cavity quantum electrodynamics extension of CIS[31,32] has allowed for investigations into plasmonic molecules under strong light–matter coupling conditions.

The rest of this manuscript is organized as follows. In Section 2, we describe the computational methods used in this study. In Section 3, we discuss the results of our calculations, including the absorption spectra of the naphthalene monomer, naphthalene dimer, and naphthalene in optical cavities. Finally, we summarize in Section 4.

2 Methods

The absorption spectra of naphthalene without strong light–matter coupling are calculated using standard quantum chemistry methods. We first investigate the naphthalene monomer to understand its plasmon-like behaviors. The geometry of the monomer is optimized using the hybrid B3LYP density functional[33,34] and Dunning's correlation consistent polarized valence double-zeta (cc-pVDZ) basis set[35] (see Table S1 of the ESI†). No further geometry optimization is performed for the remaining calculations. The naphthalene molecule is placed on the x–y plane with the long (short) molecular axis parallel to the x (y) axis; this molecular orientation is adopted for all the calculations in this work. To study the effects of intermolecular interactions, we consider a naphthalene dimer system, where two naphthalene molecules are placed along the x, y, and z directions (Fig. 1a). We adjust the intermolecular distance between the geometric centers of two monomers to control the interaction strength. The shortest dimer distances tested in this work are 8 Å in the x and y directions and 4 Å in the z direction. Even at the shortest distances, we do not observe significant differences in the dimer absorption spectra with and without geometry optimization (see Fig. S1 of the ESI†), justifying the use of unoptimized geometries in dimer calculations. The plasmon hybridization model[36,37] is used as an intuitive tool to understand the plasmon response to intermolecular interactions (see schematic illustration in Fig. 1b and discussions in Section 3.2). The absorption spectra of both naphthalene monomer and dimer systems are obtained using CIS/cc-pVDZ. As the simplest wavefunction method for computing excited states, CIS is only appropriate for transitions dominated by single excitations. In fact, quantum chemists have long known that CIS typically overestimates excitation energies by about 1 eV.[38–40] Even though it may not fully capture electron correlation effects in intermolecular interactions, this level of theory should be adequate for our study because we are only interested in a qualitative analysis of the plasmon behaviors under various conditions.

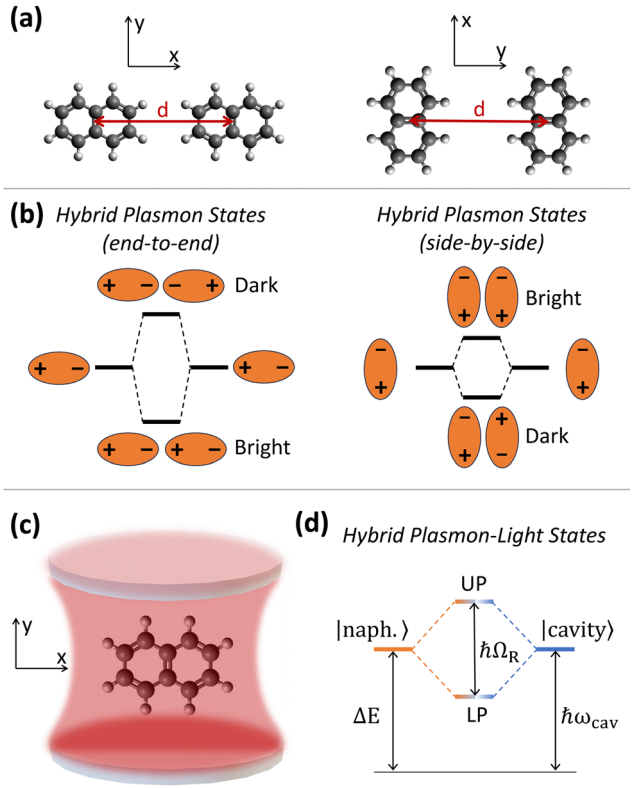

Fig. 1 Schematic representations of the systems involved in this work. (a) Naphthalene dimer placed along the x (left panel) and y (right panel) directions with distance d; each molecule's long (short) axis is parallel to the x (y) axis. (b) Hybrid plasmon states resulted from naphthalene dimer interactions along the long (left) and short (right) molecular axes, with a bright in-phase mode and a dark out-of-phase mode in each situation. (c) An encapsulated naphthalene in an optical cavity. (d) Upper polariton (LP) and lower polariton (LP) states resulted from the coupling between the naphthalene molecule and the cavity, with ΔE denoting the excitation energy of naphthalene in the absence of the cavity, ω_{cav} the cavity frequency, and Ω_R the Rabi frequency.

Strong light–matter coupling for a naphthalene molecule in an optical cavity is described using quantum electrodynamics configuration interaction with single excitations (QED-CIS). Note that QED-CIS methods inherit the limitations of the standard CIS and may not adequately describe high-order cavity effects, such as multi-photon excitations. They are, however, useful in providing a qualitative description for hybrid light–matter states known as polaritons. Here we adopt explicitly the QED-CIS-1 method proposed by McTague *et al.*[31,32] to provide a correlated treatment of the electron–photon interaction. In QED-CIS-1, the wavefunction of the electronic system coupled to a single-mode cavity is given by

$$|\Psi\rangle = c_0^0|\Phi_0\rangle \otimes |0\rangle + c_0^1|\Phi_0\rangle \otimes |1\rangle + \sum_{i,a} c_{ia}^0|\Phi_i^a\rangle \otimes |0\rangle + \sum_{i,a} c_{ia}^1|\Phi_i^a\rangle \otimes |1\rangle, \quad (1)$$

where $|\Phi_0\rangle$ and $|\Phi_i^a\rangle$ are the reference and singly-excited electronic determinants, respectively. The photon-number states $|0\rangle$ and $|1\rangle$ correspond respectively to the zero- and

single-photon states in the cavity mode. The expansion coefficients c are determined by solving a matrix eigenvalue problem of the Pauli–Fierz (PF) Hamiltonian in the length gauge and within the dipole and Born–Oppenheimer approximations,

$$\hat{H}_{\mathrm{PF}} = \hat{H}_{\mathrm{e}} + \omega_{\mathrm{cav}}\hat{b}^{\dagger}\hat{b} - \sqrt{\frac{\omega_{\mathrm{cav}}}{2}}(\lambda\cdot\hat{\mu})\left(\hat{b}^{\dagger}+\hat{b}\right) + \frac{1}{2}(\lambda\cdot\hat{\mu})^2, \quad (2)$$

where $\hat{H}_{\mathrm{e}}$ denotes the standard electronic Hamiltonian within the Born–Oppenheimer approximation, ω_{cav} is the frequency of the cavity mode, $\hat{b}^{\dagger}(\hat{b})$ is the photonic creation (annihilation) operator, λ is the coupling strength, and $\hat{\mu}$ is the dipole operator. Besides the bare electronic Hamiltonian (the first term), $\hat{H}_{\mathrm{PF}}$ contains the Hamiltonian for the bare cavity mode (the second term) and two terms that arise from the light–matter interactions, *i.e.* the bilinear coupling term (the third term) and the dipole self-energy term (the last term). Given the wavefunction for excited state I, the polarization-averaged oscillator strength in the length gauge is calculated as

$$f_I = \frac{4}{3}\omega_I \sum_{\xi=(x,y,z)} \left|\langle \Psi_I|\mu_\xi|\Psi_0\rangle\right|^2, \quad (3)$$

where ω_I is the frequency of the I-th excited state, and μ_ξ is the dipole operator in the ξ direction. We then obtain absorption spectra by convoluting the oscillator strengths with Gaussians with a full width at half maximum (FWHM) of 0.1 eV. For certain light–matter coupling strengths, we also calculate the electronic weights, which provide insights into the nature of the hybrid excited states. The electronic weight for a state is defined as the norm of the electronic part of the QED-CIS-1 expansion vector $\boldsymbol{c}$,

$$w^{\mathrm{e}} = \sqrt{\frac{\sum_{\mu}(c_{\mu}^{0})^2}{||c||^2}}. \quad (4)$$

In cavity calculations, we place the naphthalene molecule on the x–y plane, while polarizing the cavity in the x, y, and z directions (Fig. 1c). The cavity frequency (ω_{cav}) is scanned from 0 to 30 eV to cover the main absorption peaks of naphthalene. The coupling strength (λ) is tuned from 0.01 to 0.05 atomic unit (a.u.), which is an accessible range in current experiments.[41] These cavity parameters are manipulated to study the influence of strong light–matter coupling on molecular plasmons. A schematic representation of the coupling between naphthalene's plasmonic state and the cavity mode is shown in Fig. 1d, where the cavity frequency is near-resonant with the molecular excitation energy (ΔE). With an appropriate cavity polarization and coupling strength, this leads to the formation of two hybrid light–matter states, *i.e.* upper polariton (UP) and lower polariton (LP) states, separated by the Rabi splitting energy ($\hbar\Omega_{\mathrm{R}}$).

Besides investigating the separate effects of intermolecular interactions and strong light–matter coupling on molecular plasmons, we also combine the two types of interactions to study their joint influence. The absorption spectra of the naphthalene dimer in a cavity are calculated using QED-CIS-1. Given the relatively high computational cost, we use the STO-3G minimal basis set[42] to demonstrate such joint effects for a specific configuration, *i.e.* the naphthalene dimer placed along the x direction (end-to-end) in the x-polarized cavity. The dimer distance is set to 8 Å, and the cavity frequency is tuned to 8.6 eV to be near resonant with the plasmon peak of the naphthalene dimer. We vary the coupling strength from 0.01 to 0.05 a.u. to further explore the tunability of the plasmon peak under the combined interactions. To ensure a fair comparison to the non-cavity results, we recalculated the absorption spectra for the naphthalene dimer in the absence of the cavity at the CIS/STO-3G level of theory.

All non-cavity calculations (without strong light–matter coupling) are performed using the ORCA quantum chemistry package.[43] The calculations in cavities are performed using a developer version of the PySCF program,[44,45] where QED-CIS-1 is implemented based on ref. 32. Molecular orbitals and transition densities are visualized with VESTA.[46]

3 Results and discussion

3.1 Naphthalene monomer

The absorption spectrum of naphthalene (no cavity) is shown in Fig. 2a. As the most distinguished feature, the peak located at 7.33 eV is more than twenty times stronger than other peaks. The corresponding excited state arises from the constructive interaction of two single-particle transitions, *i.e.* HOMO−1 to LUMO and HOMO to LUMO+1, with equal weights of 0.47 (see Fig. 2b for the molecular orbitals). This peak is thus identified as the molecular plasmon peak due to its plasmon-like character. The peak intensity is dominated by its x-polarized component. This is because the transition density of the molecular plasmon state is polarized in the longitudinal molecular axis (x axis), shown in Fig. 2c.

We also note two other weak peaks called p-band peaks, including the lowest peak at 5.21 eV that corresponds to the HOMO to LUMO transition (weight = 0.75) and the peak at 7.49 eV (at the right shoulder of the plasmon peak) that corresponds to the HOMO−1 to LUMO+1 transition (weight = 0.70).

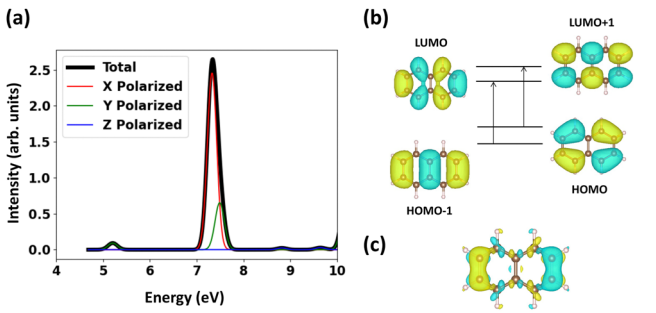

Fig. 2 (a) Polarization-averaged (black curve) absorption spectrum of naphthalene with polarized contributions in x (red curve), y (green curve), and z (blue curve) directions. Intensities are shown in arbitrary units. (b) Molecular orbitals involved in the largest two single-particle transitions that contribute to the plasmon peak. (c) Transition density of the plasmon peak.

Both peaks feature a transition density polarized in the y direction and thus have intensities dominated by the y-polarized components. Our calculations of the naphthalene monomer agree qualitatively well with the literature results.[15,16]

3.2 Naphthalene dimer

The plasmon response to dimer interactions can be described by the so-called plasmon hybridization model.[36,37] Coupling between the plasmons of the dimer will lead to a bright in-phase mode and a dark out-of-phase mode under linearly polarized light (Fig. 1b). The dark state refers to a forbidden transition under the selection rules, and therefore cannot be detected through optical absorption. Plasmon absorption peaks with a transition dipole perpendicular to the interaction axis will blue-shift as the dimer moves closer (side-by-side orientation, see the right panel of Fig. 1b), while those with a transition dipole parallel to the interaction axis will red-shift (end-to-end orientation, see the left panel of Fig. 1b). Next we examine absorption spectra of the naphthalene dimer with different intermolecular distances in the x, y, and z directions, shown in Fig. 3.

The change in the absorption spectrum as the naphthalene dimer approaches in the x direction is shown in Fig. 3 (top panel). Since the plasmon state of naphthalene features a transition dipole along the long molecular axis (x axis), we indeed observe a red-shift of the plasmon peak as the intermolecular distance decreases, consistent with the prediction of the plasmon hybridization model. The plasmonic coupling shifts the peak position from 7.29 to 6.94 eV when the dimer distance changes from 15 to 8 Å. A small red-shift of 0.04 eV at 15 Å compared to the monomer peak position (7.33 eV) indicates that plasmonic coupling is negligible beyond this distance. We therefore only consider dimer interaction within 15 Å. On the other hand, the p-band peak located at the shoulder of the plasmon peak barely changed under dimer interactions along the x axis; the peak only blue-shifts from 7.50 eV to 7.54 eV. The opposite shift of the plasmon peak and the nearby p-band peak leads to the separation of the two peaks. Such separation can be useful for distinguishing plasmon-like peaks from other absorption peaks in more complex systems.

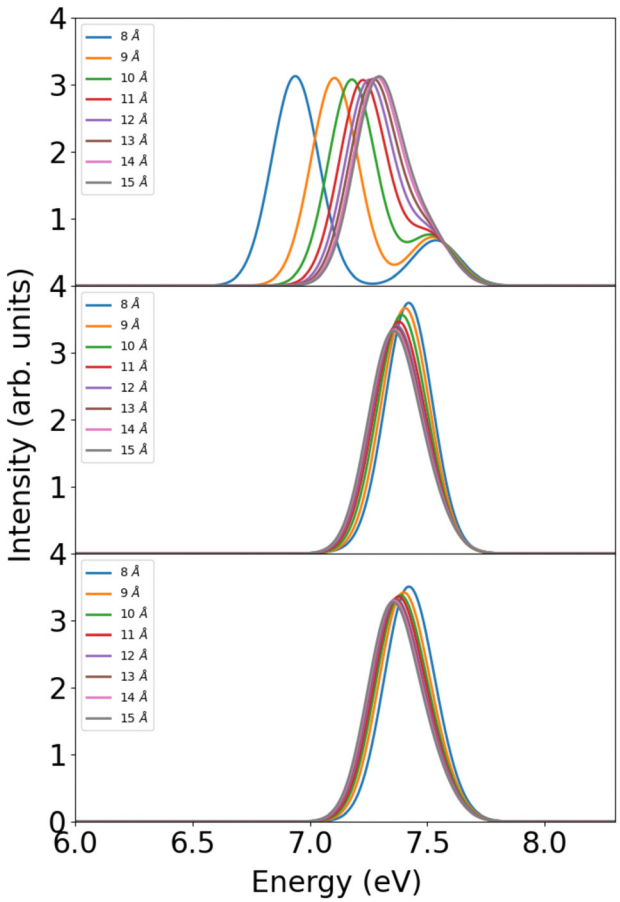

Fig. 3 Absorption spectra (in arbitrary units) of the naphthalene dimer with the inter-molecule distance ranging from 15 to 8 Å along the x (top), y (middle), and z (bottom) directions.

When the naphthalene dimer approaches in y and z directions, shown respectively in Fig. 3 middle and bottom panels, the plasmon peak undergoes a weak blue-shift with a similar magnitude (from 7.34 eV to 7.42 eV for the y direction and from 7.34 eV to 7.41 eV for the z direction). This is again consistent with the plasmon hybridization model, as the plasmonic transition dipole is perpendicular to the interaction axis (the right panel of Fig. 1b). Interestingly, the plasmon peak and the nearby p-band peak do not separate for y- and z-axis interactions, indicating a similar coupling effect for both peaks in these directions.

Comparing the extent of the shift in the plasmon peak for the x, y, and z directions, we see that the red-shift in the x direction (0.4 eV) is more pronounced than the blue-shift in the y and z directions (<0.1 eV). This is due to the fact that the plasmon state is polarized in the x direction, leading to a stronger coupling effect. Although tuning the dimer distance in the y and z directions (perpendicular to plasmon polarization) results in a smaller effect, the planar geometry of naphthalene offers a greater tunability in the z distance as close as 3–4 Å (the typical inter-layer distance in bilayer graphene[47,48]). In contrast, the dimer distance in the x direction cannot be lower than 8 Å due to steric hindrance. Fig. 4 shows the absorption spectra of the naphthalene dimer with a short intermolecular distance in the z direction. The plasmon peak is further blue-shifted from 7.42 eV to 7.68 eV as the distance decreases from 8 to 4 Å. The total shift in the z direction (from 15 Å to 4 Å) is in a similar magnitude as that in the x direction (from 15 Å to 8 Å). Overall, our findings show that tuning the intermolecular distance can effectively modulate the plasmonic response of naphthalene.

3.3 Naphthalene in optical cavities

Alternative to using intermolecular interactions as a modulator, the interaction between molecules and cavity photons offers another flexible platform to modulate molecular plasmons. As mentioned above, steric effects need to be considered when tuning the intermolecular distance. On the other hand, tuning the plasmonic response to strong light–matter interactions *via*

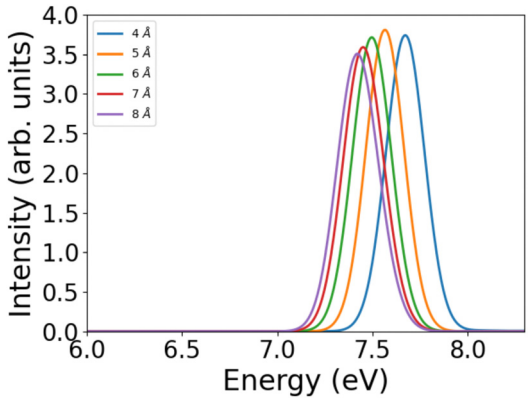

Fig. 4 Absorption spectra (in arbitrary units) of the naphthalene dimer with a short intermolecular distance ranging from 8 to 4 Å in the *z* direction.

cavity parameters (such as cavity polarization, cavity frequency, and coupling strength) could potentially circumvent some of the challenges and achieve greater plasmon modulation.

The QED-CIS-1 absorption spectra of naphthalene with a coupling strength of 0.01 a.u. and different cavity polarization directions are shown in Fig. 5. Like in naphthalene absorption spectra without cavities, the plasmon peak located at around 7.3 eV is still the main feature within the plotted energy window. Rabi splitting is clearly observed when the cavity frequency approaches the plasmon peak in the *x*-polarized cavity, but not in the *y*- and *z*-polarized cavities. This is again due to the fact that the plasmon peak is polarized in the *x* direction, as shown in Fig. 2c. A gap of 0.7 eV between the upper polariton (UP) and the lower polariton (LP) is created when the *x*-polarized cavity frequency is 7.33 eV. The *y*-polarized cavity couples to the *y*-polarized p-band peak at 7.49 eV, leading to the splitting of this weak peak (see the inset of Fig. 5 middle panel). The other p-band peak at 5.21 eV is too weak to be observed. The *z*-polarized cavity does not show any splitting of the plasmon or p-band peaks.

When we increase the coupling strength from 0.01 a.u. to a stronger regime of 0.03 and 0.05 a.u., the Rabi splitting for the plasmon peak increases significantly, as shown in Fig. 6 (upper panels). The gap between UP and LP changes from 0.7 eV to 2.1 eV and 3.1 eV, respectively. This is qualitatively consistent with the strong coupling regime where the energy splitting between the polaritons is proportional to the coupling strength.[49] The electronic weights of naphthalene with *x*-polarized cavity strength = 0.03 a.u. and 0.05 a.u. are also studied. As shown in Fig. 6 (lower panels), the plasmon peak is specifically hybridized with the photonic state to form upper and lower polaritons. Taking the LP of the plasmon state (the curved line between 6.5 and 7.5 eV) as an example, this state gains more electronic weight as the coupling strength increases from 0.03 to 0.05 a.u. However, without optical selection rules, the plasmon state is difficult to identify among other excited states in these plots, emphasizing the importance of optical absorption spectra in the study of molecular plasmons.

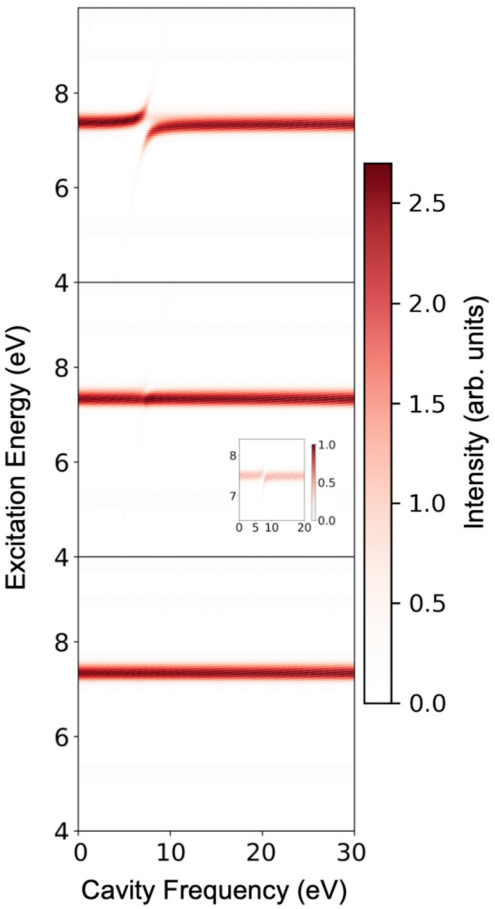

Fig. 5 Absorption spectra (in arbitrary units) of naphthalene in optical cavities polarized in the *x* (top), *y* (middle), and *z* (bottom) directions with a coupling strength of 0.01 a.u. The inset in the middle panel shows the splitting of the p-band peak at 7.49 eV in the *y*-polarized cavity, with the plasmon peak removed to reveal this subtle spectral feature.

When symmetry is allowed, one can expect that two consecutive bright states will quench within the polariton branch that connects them. In other words, under strong light–matter coupling at a certain cavity frequency, the absorption peaks of two consecutive bright states will meet and vanish completely. This is due to the destructive interference between the optical transition amplitudes from the two states connected by the polariton branch. The quenching phenomenon has been reported in a QED Bethe–Salpeter equation (QED-BSE) study of MoS_2 in an optical cavity.[27] This peculiar behavior of polariton dispersion is also observed in our calculations. Within our settings, it is easier to identify the quenching phenomenon in the *y*-polarized cavity because there are more closely lying *y*-polarized (bright) states. When the cavity is polarized in the *y* direction, the absorption peaks at 10.19 eV and 13.97 eV (both are *y*-polarized) will split as shown in Fig. 7. The UP of the 10.19 eV peak blue-shifts while the LP of the 13.97 eV peak red-shifts as the cavity frequency changes towards their average. At the cavity frequency near 12 eV, the two polaritons meet, resulting in quenching of the two consecutive bright states in the absorption spectrum.

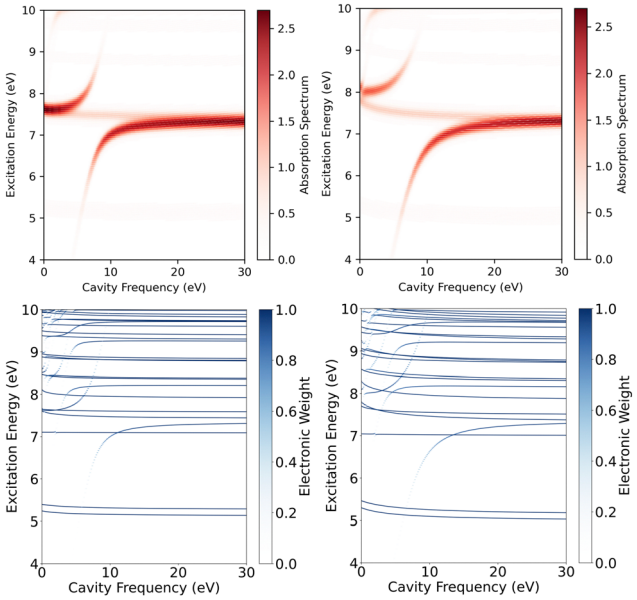

Fig. 6 Upper panel: Absorption spectra (in arbitrary units) of naphthalene in the x-polarized cavity with coupling strengths of 0.03 (left) and 0.05 (right) a.u. Lower panel: The electronic weights of naphthalene states in the x-polarized cavity with coupling strengths of 0.03 (left) and 0.05 (right) a.u.

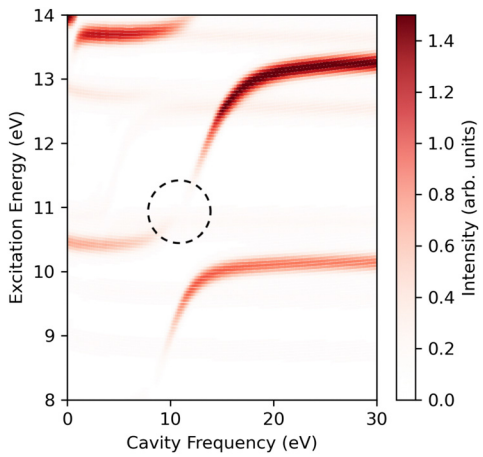

Fig. 7 Quenching of two consecutive bright states (highlighted with a circle) in the absorption spectrum (in arbitrary units) of naphthalene in the y-polarized cavity with a coupling strength of 0.05 a.u.

It is interesting to note the connections between intermolecular interactions and strong light–matter coupling as two types of modulation methods for molecular plasmons. Both methods yield two hybrid states with split energy levels analogously for the given molecular plasmon. For intermolecular interactions, the plasmonic states of the naphthalene dimer couple and result in plasmon–plasmon hybrid states (an in-phase mode and an out-of-phase mode, Fig. 1b). For strong light–matter coupling, the plasmonic state of naphthalene couples to the cavity mode and forms plasmon-light hybrid states (UP and LP, Fig. 1d). When absorption spectra are measured under linearly polarized light, an intriguing difference between the two modulation methods becomes apparent. Intermolecular interactions cause a shift of the plasmon peak position. Depending on whether the dimer is oriented end-to-end or side-by-side, one may observe red-shift or blue-shift (as elaborated in Section 3.2) since only the in-phase hybridization corresponds to an optically allowed transition. The same argument holds for the well-studied spectral shifts in molecular excitonic dimers (J- and H-aggregates).[50–52] On the other hand, strong light–matter coupling causes the plasmon peak to split into two peaks separated by the Rabi splitting energy (as discussed above), where both the UP and LP hybrid states are optically allowed.

Given the potential of intermolecular interactions and strong light–matter coupling to separately modulate molecular plasmons, it is natural to consider the combined effects of these two methods. In Fig. 8, we show the QED-CIS-1/STO-3G absorption spectra of the naphthalene dimer in an optical cavity with coupling strengths of 0.01, 0.03, and 0.05 a.u. (see more computational details in Section 2). The CIS/STO-3G absorption spectra of the dimer separated by 8 Å and 50 Å without the cavity are also shown for comparison. The use of STO-3G is justified as the spectra of the dimer without the cavity (black dashed and solid curves) qualitatively capture the main features compared to the cc-pVDZ results (Fig. 2a and Fig. 3 top panel). Here, the dimer with a 50 Å distance is used to represent the monomer spectrum as dimer interaction is negligible at this distance.

In the absence of the cavity, the plasmon peak of the dimer shifts from 9.0 eV to 8.7 eV as the distance reduces from 50 Å to 8 Å. This red-shift of 0.3 eV is consistent with the results shown in Fig. 3 (top panel). When the cavity is introduced with the dimer distance fixed at 8 Å, the plasmon peak (black solid curve) splits into two peaks (blue, orange, and green curves); Rabi splitting is 1.2 eV for λ = 0.01 a.u. (blue curve), 3.2 eV

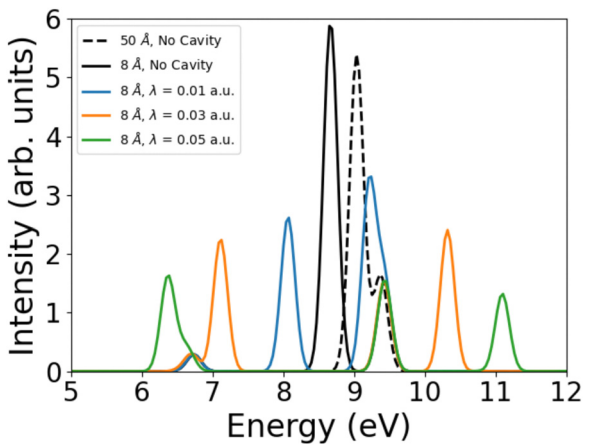

Fig. 8 Absorption spectra of the naphthalene dimer (placed along the x direction with a distance of 8 Å) in an x-polarized optical cavity with a cavity strength of 0.01 (blue curve), 0.03 (orange curve) and 0.05 (green curve). Absorption spectra of the naphthalene dimer in the absence of the cavity with a dimer distance of 8 Å (black solid curve) and 50 Å (black dashed curve) are also shown for comparison.

for λ = 0.03 a.u. (orange curve), and 4.7 eV for λ = 0.05 a.u. (green curve). Note that the p-band peak at 9.4 eV is not affected in any circumstances. The combined effects of dimer interaction and cavity coupling produce more pronounced plasmon peak shifts than either mechanism acting alone. For instance, at λ = 0.05 a.u., the LP state of the dimer plasmon in the cavity (6.4 eV) is 2.6 eV lower than the monomer plasmon peak without the cavity (9.0 eV); this red-shift is larger than the 0.3 eV shift due to dimer interaction and the 2.3 eV shift due to cavity coupling. Our results suggest that strong light–matter coupling provides an extra knob for tuning molecular plasmons and can work synergistically with intermolecular interactions.

4 Conclusions

In this study, we have successfully demonstrated the modulation of molecular plasmons in naphthalene through both intermolecular interactions and strong light–matter coupling using first principles calculations. With the CIS method, our results reveal that varying the intermolecular distance in the naphthalene dimer can significantly affect their plasmonic response. Specifically, the absorption spectra exhibit shifts in peak positions, which are dependent on the orientation and proximity of the interacting molecules. These shifts show the sensitivity of plasmonic properties to the spatial configuration of molecular systems and suggest potential avenues for tuning these properties in more complex aromatic hydrocarbons.

Furthermore, we have explored the strong light–matter coupling as a way to tune molecular plasmons by incorporating the naphthalene molecule into optical cavities. Using the QED-CIS-1 approach, we have shown that the plasmon peak of naphthalene can be effectively modulated *via* the phenomenon of Rabi splitting. The extent of this splitting was shown to be controllable by adjusting cavity parameters such as the polarization direction, cavity frequency, and coupling strength. By studying the absorption spectra of the naphthalene dimer embedded in a cavity, we have further demonstrated the combined effects of intermolecular interactions and strong light–matter coupling. Our results show that the two modulation methods can work synergistically to produce more pronounced plasmon peak shifts. This control provides a versatile platform for modulating molecular plasmons, extending beyond the capabilities of traditional chemical modifications or physical structuring alone. Moving forward, further investigations could focus on extending these modulation techniques to other plasmonic materials and exploring the potential synergistic effects of combining multiple techniques.

Author contributions

Zhen Liu: conceptualization (equal); data curation (lead); investigation (equal); software (equal); visualization (equal); writing – original draft; and writing – review & editing (supporting). Xiao Wang: conceptualization (equal); data curation (supporting); investigation (equal); software (equal); funding acquisition; software (equal); visualization (equal); supervision; and writing – review & editing (lead).

Data availability

The data supporting this article have been included as part of the ESI.†

Conflicts of interest

There are no conflicts to declare.

Acknowledgements

The authors thank A. Eugene DePrince III and Johannes Flick for helpful discussions. We acknowledge the start-up funding from the University of California, Santa Cruz and support from the Hellman Fellows Program.

References

1 X. Luo, T. Qiu, W. Lu and Z. Ni, *Mater. Sci. Eng., R*, 2013, **74**, 351–376.
2 H. Yu, Y. Peng, Y. Yang and Z.-Y. Li, *npj Comput. Mater.*, 2019, **5**, 1–14.
3 V. Amendola, R. Pilot, M. Frasconi, O. M. Maragò and M. A. Iatì, *J. Phys.: Condens. Matter*, 2017, **29**, 203002.
4 M. Dhiman, *J. Mater. Chem. A*, 2020, **8**, 10074–10095.
5 N. Zhou, V. López-Puente, Q. Wang, L. Polavarapu, I. Pastoriza-Santos and Q.-H. Xu, *RSC Adv.*, 2015, **5**, 29076–29097.
6 S. K. Cushing and N. Wu, *J. Phys. Chem. Lett.*, 2016, **7**, 666–675.
7 Z. Zhang, C. Zhang, H. Zheng and H. Xu, *Acc. Chem. Res.*, 2019, **52**, 2506–2515.
8 S. Link, M. A. El-Sayed, T. Gregory Schaaff and R. L. Whetten, *Chem. Phys. Lett.*, 2002, **356**, 240–246.
9 S. F. Tan, L. Wu, J. K. Yang, P. Bai, M. Bosman and C. A. Nijhuis, *Science*, 2014, **343**, 1496–1499.
10 K. D. Chapkin, L. Bursi, G. J. Stec, A. Lauchner, N. J. Hogan, Y. Cui, P. Nordlander and N. J. Halas, *Proc. Natl. Acad. Sci. U. S. A.*, 2018, **115**, 9134–9139.
11 A. Lauchner, A. E. Schlather, A. Manjavacas, Y. Cui, M. J. McClain, G. J. Stec, F. J. Garca de Abajo, P. Nordlander and N. J. Halas, *Nano Lett.*, 2015, **15**, 6208–6214.
12 J. B. Birks, L. G. Christophorou and R. H. Huebner, *Nature*, 1968, **217**, 809–812.
13 P. Sony and A. Shukla, *Phys. Rev. B: Condens. Matter Mater. Phys.*, 2007, **75**, 155208.
14 M. Krykunov, S. Grimme and T. Ziegler, *J. Chem. Theory Comput.*, 2012, **8**, 4434–4440.
15 E. B. Guidez and C. M. Aikens, *J. Phys. Chem. C*, 2013, **117**, 21466–21475.
16 G. U. Kuda-Singappulige, A. Wildman, D. B. Lingerfelt, X. Li and C. M. Aikens, *J. Phys. Chem. A*, 2020, **124**, 9729–9737.

17 G.-S. Park, K. S. Min, H. Kwon, S. Yoon, S. Park, J.-H. Kwon, S. Lee, J. Jo, M. Kim and S. K. Kim, *Adv. Mater.*, 2021, **33**, 2100653.
18 Y. Bao, S. Zu, Y. Zhang and Z. Fang, *ACS Photonics*, 2015, **2**, 1135–1140.
19 X.-f Hu, X.-y Zhao, Y.-w Gu, S.-p Jin, Y.-p Cui and C.-g Lu, *Sci. Rep.*, 2022, **12**, 5229.
20 M. V. Fonseca Guzman, M. E. King, N. L. Mason, C. S. Sullivan, S. Jeong and M. B. Ross, *Matter*, 2023, **6**, 838–854.
21 Z. Ma, Z. Chen, L. Zhang, X. Lu, G. Yang, X. Xu and R. Wang, *Opt. Mater. Express*, 2022, **12**, 622.
22 S. Zanotto, L. Bonatti, M. F. Pantano, V. Mišeikis, G. Speranza, T. Giovannini, C. Coletti, C. Cappelli, A. Tredicucci and A. Toncelli, *ACS Photonics*, 2023, **10**, 394–400.
23 J. Flick, M. Ruggenthaler, H. Appel and A. Rubio, *Proc. Natl. Acad. Sci. U. S. A.*, 2017, **114**, 3026–3034.
24 M. Ruggenthaler, N. Tancogne-Dejean, J. Flick, H. Appel and A. Rubio, *Nat. Rev. Chem.*, 2018, **2**, 1–16.
25 R. F. Ribeiro, L. A. Martínez-Martínez, M. Du, J. Campos-Gonzalez-Angulo and J. Yuen-Zhou, *Chem. Sci.*, 2018, **9**, 6325–6339.
26 J. Yuen-Zhou and V. M. Menon, *Proc. Natl. Acad. Sci. U. S. A.*, 2019, **116**, 5214–5216.
27 S. Latini, E. Ronca, U. De Giovannini, H. Hübener and A. Rubio, *Nano Lett.*, 2019, **19**, 3473–3479.
28 E. B. Guidez and C. M. Aikens, *Phys. Chem. Chem. Phys.*, 2014, **16**, 15501–15509.
29 E. B. Guidez and C. M. Aikens, *Nanoscale*, 2014, **6**, 11512–11527.
30 F. Alkan and C. M. Aikens, *Phys. Chem. Chem. Phys.*, 2019, **21**, 23065–23075.
31 J. McTague and J. J. Foley IV, *J. Chem. Phys.*, 2022, **156**, 154103.
32 J. J. Foley IV, J. F. McTague and A. E. DePrince III, *Chem. Phys. Rev.*, 2023, **4**, 041301.
33 C. Lee, W. Yang and R. G. Parr, *Phys. Rev. B: Condens. Matter Mater. Phys.*, 1988, **37**, 785–789.
34 A. D. Becke, *J. Chem. Phys.*, 1993, **98**, 1372–1377.
35 J. Dunning and H. Thom, *J. Chem. Phys.*, 1989, **90**, 1007–1023.
36 E. Prodan and P. Nordlander, *J. Chem. Phys.*, 2004, **120**, 5444–5454.
37 P. Nordlander, C. Oubre, E. Prodan, K. Li and M. I. Stockman, *Nano Lett.*, 2004, **4**, 899–903.
38 M. Head-Gordon, R. J. Rico, M. Oumi and T. J. Lee, *Chem. Phys. Lett.*, 1994, **219**, 21–29.
39 J. E. Subotnik, *J. Chem. Phys.*, 2011, **135**, 071104.
40 P.-F. Loos, A. Scemama and D. Jacquemin, *J. Phys. Chem. Lett.*, 2020, **11**, 2374–2383.
41 J. Flick, N. Rivera and P. Narang, *Nanophotonics*, 2018, **7**, 1479–1501.
42 W. J. Hehre, R. F. Stewart and J. A. Pople, *J. Chem. Phys.*, 1969, **51**, 2657–2664.
43 F. Neese, F. Wennmohs, U. Becker and C. Riplinger, *J. Chem. Phys.*, 2020, **152**, 224108.
44 Q. Sun, T. C. Berkelbach, N. S. Blunt, G. H. Booth, S. Guo, Z. Li, J. Liu, J. D. McClain, E. R. Sayfutyarova, S. Sharma, S. Wouters and G. K.-L. Chan, *WIREs Comput. Mol. Sci.*, 2018, **8**, e1340.
45 Q. Sun, X. Zhang, S. Banerjee, P. Bao, M. Barbry, N. S. Blunt, N. A. Bogdanov, G. H. Booth, J. Chen, Z.-H. Cui, J. J. Eriksen, Y. Gao, S. Guo, J. Hermann, M. R. Hermes, K. Koh, P. Koval, S. Lehtola, Z. Li, J. Liu, N. Mardirossian, J. D. McClain, M. Motta, B. Mussard, H. Q. Pham, A. Pulkin, W. Purwanto, P. J. Robinson, E. Ronca, E. R. Sayfutyarova, M. Scheurer, H. F. Schurkus, J. E. T. Smith, C. Sun, S.-N. Sun, S. Upadhyay, L. K. Wagner, X. Wang, A. White, J. D. Whitfield, M. J. Williamson, S. Wouters, J. Yang, J. M. Yu, T. Zhu, T. C. Berkelbach, S. Sharma, A. Y. Sokolov and G. K.-L. Chan, *J. Chem. Phys.*, 2020, **153**, 024109.
46 K. Momma and F. Izumi, *J. Appl. Crystallogr.*, 2011, **44**, 1272–1276.
47 M. S. Alam, J. Lin and M. Saito, *Jpn. J. Appl. Phys.*, 2011, **50**, 080213.
48 Y. Fukaya, Y. Zhao, H.-W. Kim, J. R. Ahn, H. Fukidome and I. Matsuda, *Phys. Rev. B*, 2021, **104**, L180202.
49 E. Orgiu, J. George, J. A. Hutchison, E. Devaux, J. F. Dayen, B. Doudin, F. Stellacci, C. Genet, J. Schachenmayer, C. Genes, G. Pupillo, P. Samorì and T. W. Ebbesen, *Nat. Mater.*, 2015, **14**, 1123–1129.
50 M. Kasha, *Radiat. Res.*, 1963, **20**, 55–70.
51 M. Kasha, H. R. Rawls and M. A. El-Bayoumi, *Pure Appl. Chem.*, 1965, **11**, 371–392.
52 P. K. Jain, S. Eustis and M. A. El-Sayed, *J. Phys. Chem. B*, 2006, **110**, 18243–18253.